A unified mechanism of O_2 reduction in aprotic Li^+- electrolytes and its consequences for Li-O_2 batteries

Lee Johnson[1,6‡], Chunmei Li[1,2‡], Zheng Liu[1,6], Yuhui Chen[1,6], Stefan A. Freunberger[3], Praveen C. Ashok[4], Bavishna B. Praveen[4], Kishan Dholakia[4], Jean-Marie Tarascon[5], Peter G. Bruce[6*]

1 EastChem, School of Chemistry, University of St Andrews, North Haugh, St Andrews, Fife, KY16 9ST, UK

2 Laboratoire de Réactivité et Chimie des Solides — UMR CNRS 6007, 33 rue Saint-Leu, 80039 Amiens Cedex, France

3 Christian Doppler Laboratory for Lithium Batteries, and Institute for Chemistry and Technology of Materials, Graz University of Technology, Stremayrgasse 9, 8010 Graz, Austria

4 SUPA, School of Physics & Astronomy, University of St Andrews, North Haugh, St Andrews, Fife, KY16 9SS, UK

5 Collège de France, 11 place Marcelin Berthelot, 75231 Paris Cedex, France

6 Departments of Materials and Chemistry, University of Oxford, UK

* Author to whom correspondence should be addressed

ABSTRACT

Understanding the mechanism of O_2 reduction in Li^+-containing aprotic solvents is essential to unlock the exceptional specific energy of the lithium-oxygen battery. We describe a single unified mechanism, which embraces previous models as limiting cases. O_2 reduction to form solid Li_2O_2 proceeds by an electrode surface or solution pathway depending on the influence of the solvent on the solubility of the LiO_2 intermediate, more precisely the free energy of the reaction $LiO_2^* \rightleftharpoons Li^+_{(sol)} + O_2^-{}_{(sol)}$ + ion pairs + higher aggregates (clusters). Ethers are intermediate solvents resulting in simultaneous formation of significant Li_2O_2 surface films and Li_2O_2 particles in solution at high voltages. The unified mechanism shows that low donor number solvents are likely to lead to premature cell death, whereas high donor number solvents can sustain discharge and capacities more than three times that of low donor number solvents, encouraging research on new, sufficiently stable, high donor number solvents.

The rechargeable Li-O_2 battery would transform energy storage if a significant proportion of its theoretical specific energy, which exceeds by some margin that of lithium-ion batteries, could be realized in practice[1-10]. At the positive electrode on discharge, O_2 enters the pores of the electrode where it is reduced and combines with the Li^+ ions from the electrolyte to form solid Li_2O_2. The process is reversed on charging. However, realizing these processes rapidly, efficiently, and sustainably for many cycles is a formidable challenge[11-38]. In order to overcome the challenges at the positive electrode it is essential to understand the electrochemical mechanism of O_2 reduction in Li^+ containing aprotic electrolytes.

Two different models of O_2 reduction have been proposed: one describes O_2 reduction to form Li_2O_2 as a process taking place on the electrode surface[11,12] and the other involves Li_2O_2 formation in solution (electrolyte)[14-16] and is based on the Hard Soft Acid Base Theory of Pearson[39]. The different models have very different implications for how the hurdles of achieving fast, reversible, formation and decomposition of Li_2O_2 with low polarization and sustainable cycling may be achieved.

Here we investigate O_2 reduction across a range of solvents and show that O_2 reduction can be described by a single unified mechanism, which embraces the previous models as limiting cases. At high voltages (low overpotentials) O_2 undergoes a 1 electron reduction to LiO_2 that is partitioned between LiO_2 dissolved in the electrolyte and LiO_2 adsorbed on the electrode surface, according to the equilibrium $LiO_2^* \rightleftharpoons Li^+_{(sol)} + O_2^-{}_{(sol)}$ + ion pairs + higher aggregates (* indicates surface adsorbed LiO_2). High donor number (DN) solvents result in strong solvation of Li^+ or Li^+ containing species and the equilibrium being displaced to the right resulting in mainly soluble LiO_2, whereas for low DN solvents such solvation is weaker and the equilibrium lies to the left resulting in surface adsorbed LiO_2 being dominant. In the latter case LiO_2^* then disproportionates or undergoes a 2nd reduction to Li_2O_2 on the electrode surface, whereas in the former disproportionation of LiO_2 in solution dominates, precipitating Li_2O_2.

Ethers, such as dimethoxyethane (DME), have an intermediate DN and exhibit significant contributions from both solution and surface pathways, which occur simultaneously at high voltages. At low voltages (high overpotentials), LiO_2 is transformed rapidly by a 2nd electron reduction to Li_2O_2 on the electrode surface in all solvents. We also demonstrate that the Li_2O_2 morphologies (large particles or particulate surface films) vary with solvent, in accord with the unified mechanism.

The mechanism has implications for the performance of Li-O_2 cells. The dominance of Li_2O_2 surface films in low DN solvents is likely to lead to premature cell death. In contrast, the dominance of solution Li_2O_2 growth in high DN solvents can sustain discharge and a capacity more than three times that of low DN solvents. These results encourage effort on identifying new, sufficiently stable, electrolytes based on high DN solvents for Li-O_2 batteries.

RESULTS AND DISCUSSION

We examine O_2 reduction in four solvents spanning a wider range of DNs than before and using a range of complementary techniques. We begin by presenting the electrochemical and spectroscopic data for O_2 reduction in the four solvents. This is followed by sections explaining the unified mechanism of O_2 reduction and its origin in the solubility of LiO_2, how this correlates with the solvent dependence of Li_2O_2 morphologies and the implications the mechanism has for the future of the Li-O_2 battery.

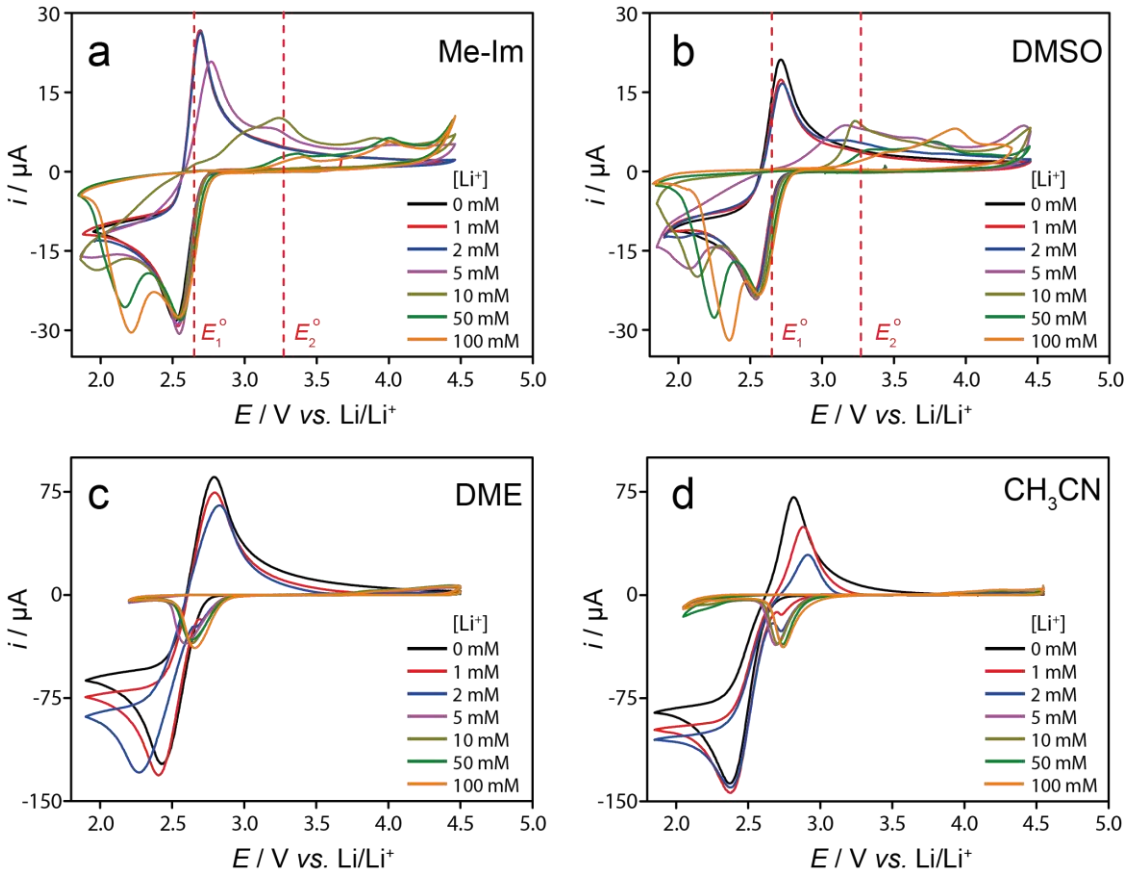

Figure 1 | CVs demonstrating the significant effect solvent donor number and cation type have on O_2 reduction. Data collected in O_2 saturated (a) Me-Im, (b) DMSO, (c) DME and (d) CH_3CN at a Au electrode with various ratios of $[Li^+]/[TBA^+]$**.** The total electrolyte concentration was 100 mM and the numbers on the plots indicate the concentrations of Li^+, where the remaining concentrations are TBA^+. The scan rate was 100 mV s^{-1} and the anion was ClO_4^-. E_1^0 and E_2^0 indicate the standard potentials for the 1st and 2nd O_2 reductions, respectively.

Comparison of CVs in the four solvents

CVs for O_2 reduction in each of the four solvents, collected at a Au electrode and over a wide voltage range, are presented in Fig. 1. This is the first report of O_2 reduction in 1-methylimidazole (Me-Im) or any solvent with such a high DN (Me-Im, 47, dimethyl sulfoxide, DMSO, 30), see Supplementary Discussion and Supplementary Fig. S1 for determination of the DN of Me-Im. For each solvent the cation is varied from 100 mM TBA^+ (tetrabutylammonium cation) to 100 mM Li^+. In the presence of only TBA^+ the CVs in all four solvents exhibit a single redox process. In contrast, in the presence of only Li^+ there is a strong dependence on the CVs with DN, high DN solvents exhibit two reduction peaks and no oxidation peaks at potential < 3 V, whereas low DN solvents exhibit one reduction peak and no oxidation, < 3 V, in accord with previous studies[14,16].

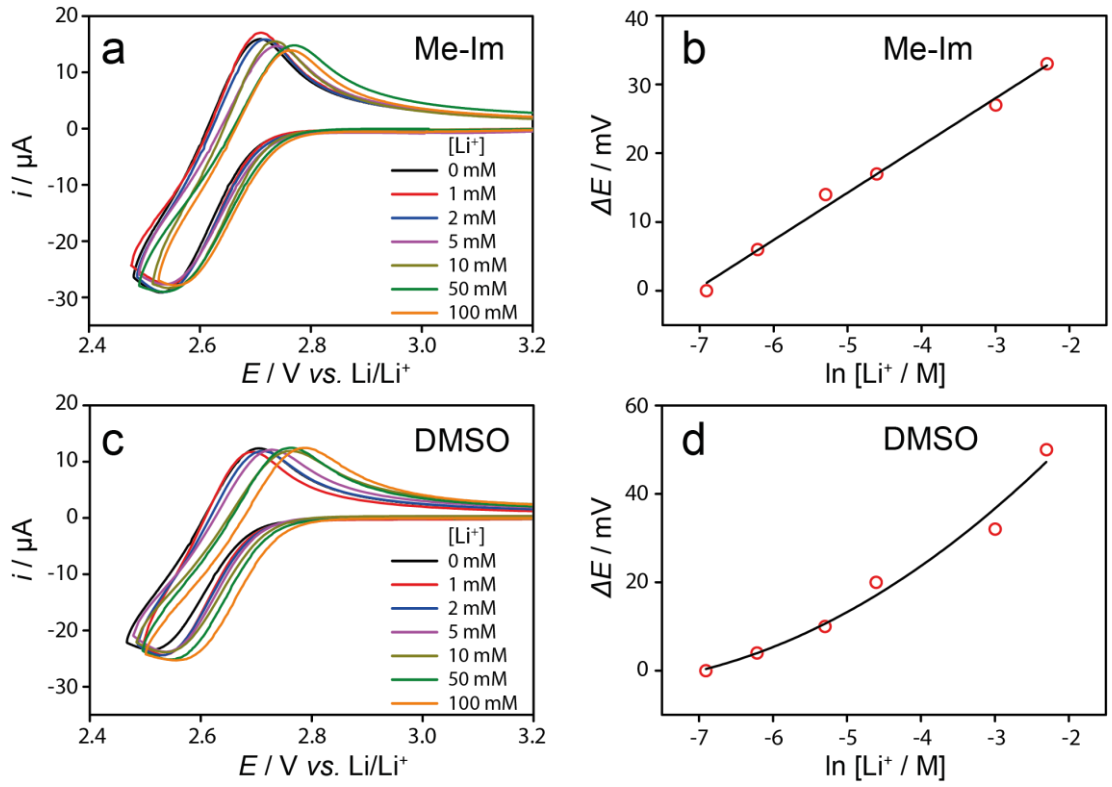

Figure 2 | (a, c) CVs showing that the first step of O_2 reduction in high donor number solvents is a reversible 1e$^-$ process in solution. Data obtained in O_2 saturated Me-Im and DMSO at a Au electrode with various ratios of $[Li^+]/[TBA^+]$ and cycled over the high voltage peak alone (see Fig. 1). The total electrolyte concentration was 100 mM in all cases and the numbers on the plot indicate the concentrations of Li^+, where the remaining concentrations are TBA^+. The scan rate was 100 mV s^{-1} and the anion was ClO_4^-. b and d show the shifts of E^0_1 (O_2/O_2^-) with $\ln[Li^+]$ concentration for Me-Im and DMSO, obtained by fitting to the CV data in a and c. Circles – experimental data, solid line – best fit.

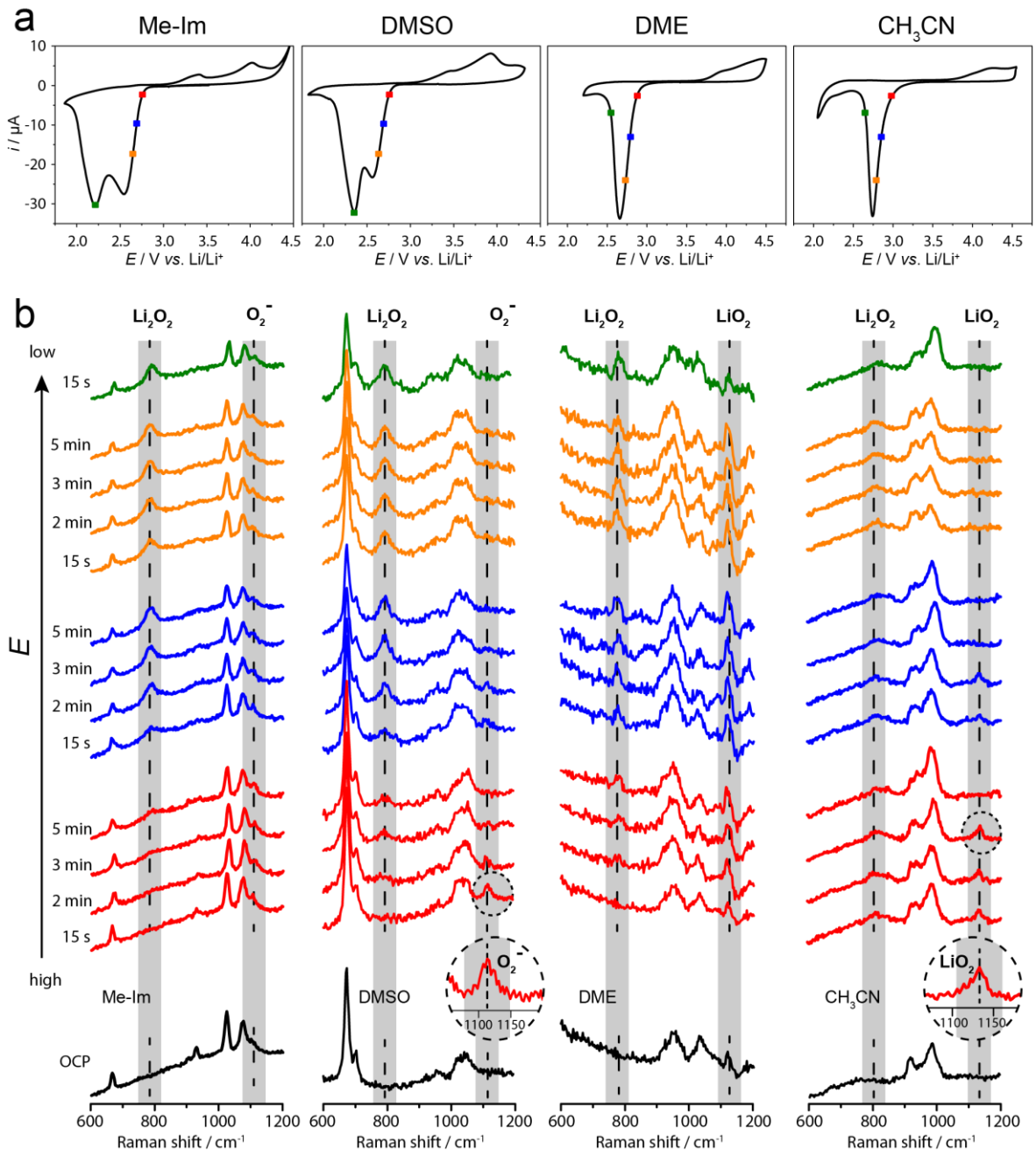

Figure 3 | SER spectra demonstrating that at high voltages (low overpotentials) O_2^- and LiO_2 species are observed on the electrode surface at short times in high and low donor number solvents respectively, to be replaced by Li_2O_2 with the passage of time. At low voltages (high overpotentials) Li_2O_2 is apparent from short times. Spectra collected at a Au electrode during O_2 reduction in the presence of 100 mM $LiClO_4$ in various aprotic solvents and recorded at different times while holding at various constant potentials indicated by the matching colored markers in the CVs above each stack of spectra. Vertical dotted lines with grey highlighting show positions of O_2^-, LiO_2 and Li_2O_2. Insets show expanded areas of spectral regions outlined by the dashed circles. Spectra at the bottom were collected at the open circuit potential (OCP).

1-Methylimidazole (Me-Im) and dimethyl sulfoxide (DMSO)

To explore O_2 reduction in high DN solvents in more detail, CVs were collected at a Au electrode in Me-Im and DMSO and for various ratios of Li^+ to TBA^+ but now over a restricted voltage range, Fig. 2. It is well known that in TBA^+ electrolytes chemically reversible O_2 reduction to O_2^- occurs and the CVs in TBA^+ exhibit a single redox peak in accord with this[40-43]. As TBA^+ is continuously replaced by Li^+, there is little change in the CVs, Fig. 2, only a relatively small continuous shift to more positive potentials. In all cases the CVs fit a 1 electron redox process of freely diffusing species, Supplementary Fig. S2, suggesting that on O_2 reduction, O_2^- is dissolved in solution in the presence of Li^+ (i.e. LiO_2 is soluble), rather than being confined to the electrode surface. The small differences in the magnitudes of the shifts in the standard potential between DMSO and Me-Im are considered in the Supplementary Discussion.

The potentials in Fig. 2 are below the thermodynamic potential for Li_2O_2 formation, therefore spontaneous disproportionation of O_2^- to form Li_2O_2 is expected[2,14]. This is observed on reducing the scan rate from 100 mV s^{-1} to 5 mV s^{-1}; the area of the backward (anodic) peak is now lower than the forward (cathodic) peak, consistent with an EC mechanism, i.e. a chemical step following the 1 electron reduction of O_2 to O_2^-, Supplementary Fig. S3, which removes the product of reduction, O_2^- so that it is less available for subsequent oxidation. Fitting the CVs at this scan rate provided a first-order rate constant for the disproportionation in DMSO of 0.03 s^{-1}, in satisfactory agreement with the value obtained for the same reaction carried out homogeneously using KO_2 in solution, 0.07 s^{-1} (see Supplementary Discussion and Supplementary Fig. S4). 100 mV s^{-1} is sufficiently fast compared with the rate of disproportionation such that disproportionation is not observed at that scan rate. Note that the 1 electron reduction of O_2 ($1e^-/O_2$) cannot be detected by Differential Electrochemical Mass Spec (DEMS) because the following chemical reaction, $2LiO_2 = Li_2O_2 + O_2$, generates O_2 resulting in a net $2e^-/O_2$ ratio and the lifetime of LiO_2 in solution is too short compared with the time to detect the mass changes in DEMS.

Based on the standard potential for the overall formation of Li_2O_2 ($2Li + O_2 \rightleftharpoons Li_2O_2$; $E^0 = 2.96$ V)[44] and for the 1st reduction of O_2 to O_2^- ($E^0_1 = 2.65$ V), the standard potential for the 2nd reduction O_2^- to Li_2O_2, E^0_2, is located at 3.27 V[45], therefore, thermodynamically the 2nd reduction to form Li_2O_2 should occur immediately upon the 1st. However, as observed in Fig. 1, a 2nd reduction peak, associated with Li_2O_2 formation, occurs at a significantly lower potential than the 1st, therefore the 2nd reduction contributes little to the current at high potentials. Indeed, if this were not the case we would not observe the chemically reversible 1 electron reduction of O_2 to O_2^- in solution noted above. Also evident in Fig. 1, is a strong dependence of the 2nd reduction peak on the Li^+ concentration, the position changing by 300 mV in DMSO on varying the lithium concentration between 1 to 100 mM. In other words Li^+ is directly involved in the 2nd reduction step.

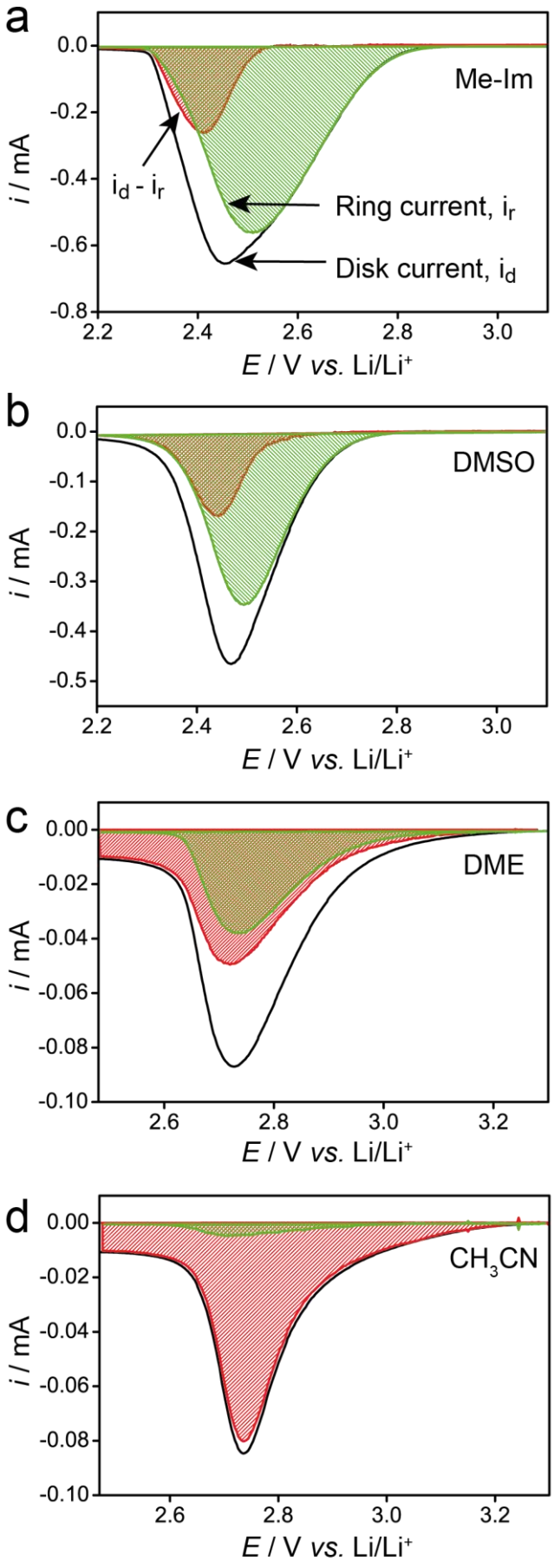
a
Me-Im
$i_d - i_r$
Ring current, i_r
Disk current, i_d
i / mA
E / V vs. Li/Li+
b
DMSO
i / mA
E / V vs. Li/Li+
c
DME
i / mA
E / V vs. Li/Li+
d
CH3CN
i / mA
E / V vs. Li/Li+

Figure 4 | Evidence from rotating ring-disk experiments showing the presence of O_2^- in solution in high donor number solvents (Me-Im and DMSO), some in the intermediate donor number solvent (DME) and essentially none in low donor number CH_3CN. Polarization curves obtained in O_2 saturated (a) Me-Im, (b) DMSO, (c) DME and (d) CH_3CN containing 100 mM $LiClO_4$ (black line) disk current i_d, (green area) ring current i_r and (red area) $i_d - i_r$. The RRDE was a 5 mm diameter Au disk with a GC ring and the rotation rate was 2000 RPM.

While electrochemical data are valuable, *in situ* electrochemical surface enhanced Raman spectroscopy (SERS) provides direct evidence for the species on the electrode surface and in concert with the other techniques provides evidence for the mechanism of O_2 reduction, Fig. 3. Beginning with DMSO, SERS reveals that there is no evidence of LiO_2 on the electrode surface at any potential during O_2 reduction, thus demonstrating that the surface model does not apply since it predicts formation of LiO_2* on the electrode surface as an intermediate, Fig. S5[11]. At high potentials (red and blue spectra in Fig. 3) and short times, formation of O_2^- on the electrode surface is observed exactly in accord with a solution model. Indeed, these spectra are indistinguishable from that obtained in a solution of $TBAClO_4$, Fig. S5. Rotating ring-disk electrode (RRDE) studies, where O_2 is reduced at the disk and O_2^- detected at the ring, as explained in the Methods section, show a one-to-one ratio of O_2 generation to O_2^- collection at these same potentials, confirming the formation of O_2^- as a relatively stable species in solution, Fig. 4. Even at the highest potential some Li_2O_2 is observed in the SERS after several minutes. This may be due to the 2nd reduction, which, as noted above, is thermodynamically allowed (and hence must occur) at all potentials below E^0 for Li_2O_2 formation, although its contribution to the current is small at these high potentials, Fig. 1. Alternatively, disproportionation near the surface and subsequent nucleation and growth of Li_2O_2 on the surface could account for the Li_2O_2 in the SERS at long times. As the Li_2O_2 grows on the electrode it reduces the free surface available for O_2^- adsorption, resulting in the O_2^- peak reducing in intensity with time (see red spectra). At lower potentials (green spectrum in Fig. 3), corresponding to the region of the second reduction peak in the CVs, Fig. 1, there is clear evidence of Li_2O_2 in SERS after the shortest time. At these low potentials, the second reduction is fast and follows immediately after the first, leading to rapid formation of Li_2O_2 on the electrode surface. In addition, RRDE measurements show a deviation from a 1 electron reduction to a 2 electron reduction at comparable potentials, confirming the mechanism, Fig. 4. The SERS in Me-Im are consistent with DMSO, however, a solvent peak in the region of O_2^- and LiO_2 makes the analysis less clear.

The maximum Li^+ concentration used in Fig. 1 is 0.1 M. Extending to higher Li^+ concentrations continues the trend seen in Fig. 1. The 2nd peak moves to yet higher potentials with increasing Li^+ concentration in Me-Im and DMSO, Supplementary Fig. S6, in accord with the 2nd reduction being dependent on Li^+ concentration. RRDE measurements at

0.5 M, Supplementary Fig. S7, confirm that O_2^- is still formed in solution at these higher Li^+ concentrations.

Acetonitrile (CH_3CN)

The CVs in Fig. 1 for acetonitrile (CH_3CN, DN 14) exhibit an abrupt change as TBA^+ is replaced by Li^+, with the appearance of a new reduction peak at higher potentials, which grows in intensity with increasing Li^+ concentration, rather than the continuous shift of the redox peak observed in high DN solvents. The position of this new peak, more positive of the reversible O_2 reduction peak, is consistent with the formation of a more stable discrete species as proposed by Luntz[11].

The *in situ* SERS, Fig. 3, provides direct evidence that the surface mechanism dominates in low DN solvents. We have reported SERS in CH_3CN before, but here we have carried out new experiments under identical conditions to the other solvents to provide a direct comparison[46]. SERS shows that there is no evidence of O_2^- on the surface at any potential, instead LiO_2 is present. This is consistent with the surface mechanism and NOT the solution mechanism. RRDE measurements also confirm the absence of all but a very small contribution from O_2^- in solution, Fig. 4. The SERS data reveal that the rate of transfer of LiO_2* to Li_2O_2 increases significantly at lower potentials. LiO_2* can transform to Li_2O_2* on the electrode surface by disproportionation and/or a 2nd electron transfer. Lower potentials will increase the surface concentration of LiO_2* and hence the rate for disproportionation, while at the same time increasing the overpotential driving the rate of the 2nd reduction.

Extending the Li^+ concentration range beyond 0.1 M has no significant effect on the electrochemistry in CH_3CN, Supplementary Fig. S6, in contrast to high DN solvents. RRDE measurements confirm the absence of O_2^- in solution.

Dimethoxyethane (DME)

CVs for O_2 reduction in DME with varying TBA^+/Li^+ ratios are shown in Fig. 1. They resemble those observed for low DN solvents, such as CH_3CN. Due to a solvent peak in the SERS overlapping with the expected O_2^- and LiO_2 peaks, we could not confirm the nature of the superoxide species, Fig. 3, but *in situ* SERS does confirm the growth of Li_2O_2, although more slowly than in CH_3CN. While the CVs point to a surface model, RRDE measurements reveal a significant concentration of O_2^- in solution in the same potential range, green region in Fig. 4. The DN of DME (DN 20) lies between that of DMSO (DN 30) and CH_3CN (DN 14). Previous authors have recently interpreted the switch from large Li_2O_2 particles at high voltages/low currents to surface films at low voltages/high currents, as implying LiO_2 solubility in ethers[21]. The present results are in accord with this, they provide specific evidence for the presence

of O_2^- in solution at high potentials in DME. However, in addition we identify that both pathways, solution and surface, operate simultaneously at high potentials, consistent with the observations of surface films and particles of Li_2O_2 at the same potential/current (discussed below and in Fig. 7).

The above studies combining electrochemical and spectroscopic methods, demonstrate that O_2 reduction to Li_2O_2 involves LiO_2 as an intermediate dissolved in solution in high DN solvents passing to LiO_2 on the electrode surface with decreasing solvent DN.

Which pathway solution or surface?

Previously, the hard soft acid-base theory of Pearson was invoked to explain the existence of a solution mechanism for O_2 reduction in aprotic solvents containing Li^+ ions[14]. Li^+ ions in high and low DN solvents were considered to be soft and hard acids respectively. However, all solvated Li^+ ions (typically a Li^+ ion is surrounded by 4 solvent molecules)[47] might be expected to be relatively polarizable and hence soft, irrespective of whether the DN of the solvent is high or low. Here we offer an interpretation of O_2 reduction in aprotic solvents containing Li^+ ions based on the solubility of LiO_2.

Considering first the mechanism of O_2 reduction at high voltage (low overpotential). Based on combining all the experimental data presented above, on O_2 reduction in all solvents the first step involves O_2 undergoing a 1 e^- reduction to form LiO_2, which is distributed between LiO_2 adsorbed on the electrode surface and LiO_2 dissolved in the adjacent electrolyte, according to the equilibrium:

$$LiO_2^* \rightleftharpoons Li^+_{(sol)} + O_2^-{}_{(sol)} + \text{ion pairs} + \text{higher aggregates (clusters)} \qquad (1)$$

Note the equation simply indicates an equilibrium between adsorbed LiO_2 and LiO_2 dissolved in solution. As is typical in aprotic solvents, free ions, ion pairs, as well as higher aggregates (clusters) are all possible species in solution[48,49]. In high DN solvents, we observe experimentally mainly LiO_2 dissolved in solution, therefore the Gibbs free energy for the dissolved LiO_2 is lower than LiO_2* on the electrode surface and the equilibrium lies to the right, with reduction proceeding predominantly by the solution pathway. In low DN solvents, where we observe mainly LiO_2 on the electrode surface, the Gibbs free energy for LiO_2* on the surface is lower than LiO_2 dissolved in solution and the equilibrium lies to the left of equation (1) with the surface pathway dominating, Fig. 5. The trend with DN is in accord with the cation solvation being a major determinant of the solubility of LiO_2, high DN promoting strong solvation and LiO_2 dissolution.

The mechanism of O_2 reduction and equation (1) presented in this paper arise solely from the experimental data. However, the values for ΔG^0, and hence predictions of the position of the equilibrium in each solvent, may be estimated somewhat approximately by

combining the Gibbs free energies of the following reactions (equations 2 + 3 + 4 = equation 1):

$$O_{2(sol)} + Li_{(s)} \rightleftharpoons O_2^-{}_{(sol)} + Li^+{}_{(sol)} + \text{ion pairs} + \text{higher aggregates (clusters)} \quad (2)$$

$$O_{2(g)} \rightleftharpoons O_{2(sol)} \quad (3)$$

$$LiO_{2(s)} \rightleftharpoons O_{2(g)} + Li_{(s)} \quad (4)$$

The experimental details of how the free energies of the three equations were obtained are given in the Supplementary Discussion. The values of ΔG^0 for equation (1) are given in Fig. 5 and correctly predict the trend from a solution dominated to a surface dominated pathway as the DN decreases. The values derived for ΔG^0 of equation (1) can only be considered as a rough approximation. In the absence of data for the ΔG^0 of LiO_2* adsorption we used the value for the formation of solid LiO_2, but we cannot be certain that the state of LiO_2 on the surface is similar to that of a solid film. The ΔG^0 values for equation (2) are also only approximations as they are based on measuring the O_2/O_2^- and Li/Li^+ redox couples

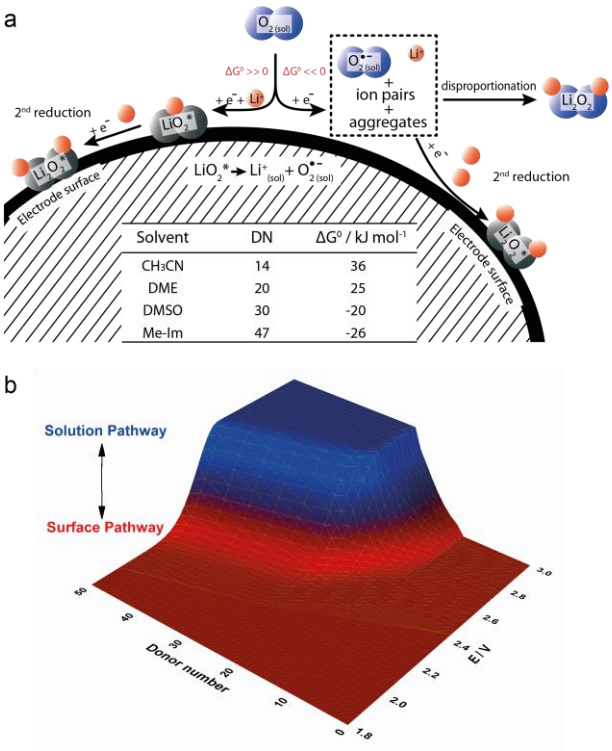

Figure 5 | (a) Schematic of the O_2 reduction mechanism in an aprotic solvent containing Li^+ showing the surface pathway followed when ΔG^0 >> 0 (low DN) and the solution pathway followed when ΔG^0 << 0 (high DN), ΔG^0 refers to equation (1), also shown above. The table shows the estimated ΔG^0 for equation (1) in solvents with various DNs. (b) Plot showing the dominant pathway as a function of DN and potential. O_2 reduction in high DN solvents and at high potentials (low overpotentials) follows the solution pathway (blue) and at low potentials (high overpotentials) the surface pathway (red). O_2 reduction in low DN solvents at all potentials follows the surface pathway (red).

separately. The former redox couple is measured in each of the four solvents containing $TBAClO_4$ and the latter in each of the four solvents containing $LiClO_4$. The ΔG^0 for LiO_2 dissolved in each of the four solvents containing $LiClO_4$ (the situation that arises on O_2 reduction) cannot be identical because of differences in ion-ion interactions (ion association) between solutions used for the Li/Li^+ and O_2/O_2^- redox couples (equation 2) and dissolved LiO_2 (equation 1), for example dissolved LiO_2 includes Li^+ - O_2^- interactions that are absent when the couples are measured separately. However, despite these approximations the estimated Gibbs free energies for equation (1) are in good agreement with the experimental evidence, predicting the correct trend from solution dominated (negative ΔG^0) to surface dominated (positive ΔG^0) pathways and hence suggesting that the free energies for equations (2-4) do capture the main contributions to the energetics of equation (1), and are reasonable approximations. This is because the ion-solvent rather than ion-ion interactions dominate the differences in the free energies between the different solvents, something that has to be the case since qualitatively DN does predict which solvents will dissolve LiO_2. Although ΔG^0 for DME is positive and therefore the surface pathway is significant, the value of ΔG^0 corresponds to a O_2^- concentration in solution of 0.4 mM (see Supplementary Discussion for calculation), consistent with some solution growth of Li_2O_2 and in accord with the RRDE results and the formation of large Li_2O_2 particles, as discussed later. It should be noted that equation (1) is not a step in the reduction, but simply represents the relative stability of the two possible intermediates O_2^- and LiO_2.

The solubility of LiO_2 in the electrolyte and its dependence on the nature of the solvent plays a central role in determining the position of the equilibrium in equation (1) i.e. ΔG^0, and hence whether O_2 reduction occurs predominantly in solution or on the electrode surface. Considering the solvation of dissolved LiO_2 and its dependence on the nature of the solvent. The potential for O_2/O_2^- has been reported to vary with solvent acceptor number indicating a change in O_2^- solvation with solvent[50]. For the solvents studied here we find a variation of E^0 for O_2/O_2^- of 60 mV, but the E^0 for Li/Li^+ varies more, by 520 mV from Me-Im (high DN) to CH_3CN (low DN). What these trends in E^0 for the two redox couples show is that the solvation energy of cations is highly solvent dependent and much greater in high compared with low DN solvents, and that the relative solubility of LiO_2 in the different solvents and hence position of the equilibrium in equation (1) is determined mainly by the solvation of Li^+. Of course, for the reasons mentioned above, these estimates of ion solvations are only approximations. Nevertheless, the trend to higher cation solvation with increasing DN fits well with the observed increase in LiO_2 solubility with DN. Note that we do not use DN in any estimate of solvation, recognizing that DN is only a part of what effects solvation.

In the case of solvents where LiO_2 is dissolved in solution (high DN), the second step in Li_2O_2 formation is disproportionation, Fig. 5. We do not know the detailed mechanism by which this occurs. We do know that it does occur from the sweep rate dependence of the CVs (SI page 5), which reveal a chemical step following the 1 electron reduction of O_2, and from the

fact that addition of KO_2 to a solution containing a Li^+ salt, such as $LiClO_4$, results in precipitation of Li_2O_2, which can only occur by disproportionation. The measured rate of disproportionation, 0.03 to 0.07 cm^{-1} (see SI) is in accord with the rate of precipitation of Li_2O_2. Previous modeling studies, have suggested relatively slow disproportionation of larger clusters[49,51]. However we do not know which species (ion pairs, or larger aggregates) might be involved in disproportionation. For this reason the representation of the disproportionation step in Fig. 5 simply represents that the process occurs and does not specify a particular species, other than it must involve Li^+. Considering the reduction at low potentials (high overpotentials). Based on the data presented above, at these lower potentials LiO_2 whether in solution (high DN) or on the surface (low DN) is transformed rapidly to Li_2O_2 by the 2nd electron reduction, which is fast at these potentials, forming a film of Li_2O_2 on the electrode surface regardless of the solvent DN, Fig. 5.

Consequences for Li-O_2 batteries

Although knowing the reduction mechanism is important, the consequences for Li-O_2 batteries are arguably of greater significance. In a practical cell it is desirable to operate at high potentials (low overpotentials) to ensure high efficiency (this requires good rate capability to sustain high current at such potentials). The consequences of the different Li_2O_2 formation pathways in high and low DN solvents at high potentials are demonstrated in Fig. 6, where we discharge at a planar electrode in each solvent. In low DN solvents the voltage soon decays leading to cell death, due to the Li_2O_2 film growth on the electrode. The

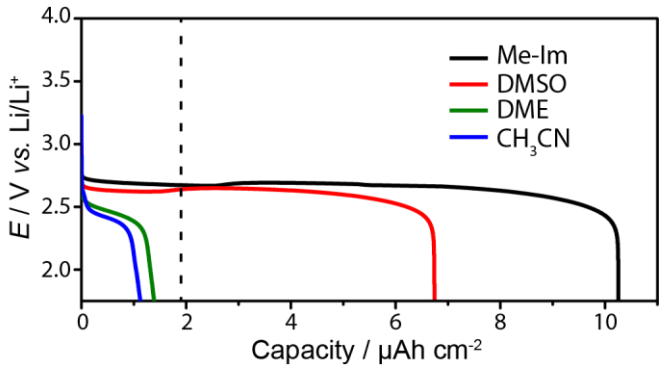

Figure 6 | Potential *vs.* time at a planar Au electrode in various O_2 saturated aprotic solvents, 100 mM $LiClO_4$ showing early cell death for low donor number solvents but sustained capacity beyond the 7 nm limit (dashed line) for a Li_2O_2 film in high donor number solvents. The discharge rate was 60 µA cm^{-2}. Note that the potentials were measured against $LixFePO_4$ in each solvent and then 3.45 V subtracted to give the potential *vs.* Li/Li^+, i.e. these are the potentials that would be exhibited by a Li-O_2 cell in each solvent. The slight drop and then rise for the potentials corresponding to the high DN solvents at the early stage of discharge, is likely to be due to nucleation and growth[52].

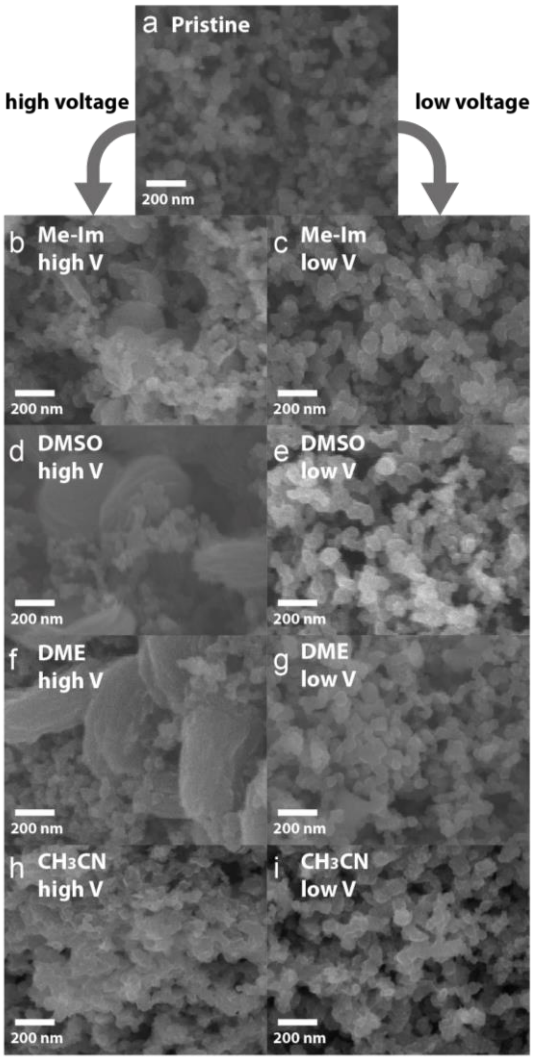

Figure 7 | SEM images showing the Li_2O_2 morphologies obtained in different solvents and at different potentials. **The morphologies are as predicted by the unified mechanism.** (a) pristine, (b, d, f, h) high (red markers in Fig. 3 CVs) and (c, e, g, i) low (green markers in Fig. 3 CVs) potentials. Porous carbon cathodes in O_2 saturated 100 mM $LiClO_4$ in the four aprotic solvents were used**.**

capacities at cell death correspond to a Li_2O_2 layer of ~5-6 nm, the thickness at which electrochemistry is expected to cease[53]. In contrast, in high DN solvents discharge continues far beyond this limit because most Li_2O_2 grows from solution, Fig. 6. Of course discharge eventually terminates even in high DN solvents, because there is always some Li_2O_2 formation on the electrode surface as noted above in the SERS results for DMSO. The intermediate DN ethers exhibit similar voltage decay to CH_3CN in Fig. 6, reflecting the significant contribution of surface Li_2O_2 films growth.

Optimized porous cathode structures for low DN (surface Li_2O_2 growth) and high DN (solution Li_2O_2 growth) solvents will be different as described in the Supplementary

Discussion, where it is shown that theoretically high DN solvents can lead to specific capacities more than three times greater than low DN solvents.

Recent important papers by several authors, including Nazar and Shao-Horn, have investigated the growth and morphology of Li_2O_2 in ethers, demonstrating significant differences in morphology with current density[21,24]. These results can now be placed in the wider context of the effect of different solvents and their different pathways of oxygen reduction (solution or surface) on the Li_2O_2 morphology. The morphologies obtained for each solvent at high and low potentials are shown in Fig. 7 and are considered in the Supplementary Discussion. The morphologies are as predicted by the mechanism. Large Li_2O_2 particles are observed in high DN solvents (Me-Im and DMSO) at high potentials (low overpotentials), film formation is observed at low potentials (high overpotentials) and in low DN solvents at all potentials. The intermediate DN DME results in Li_2O_2 films at low potentials and both films and particles at high potentials.

In conclusion, a unified mechanism of O_2 reduction in aprotic solvents is described, which embraces the two previous models, and in which the pathway of O_2 reduction to form Li_2O_2, solution or electrode surface, depends on the solubility of the LiO_2 intermediate, specifically the free energy of the reaction $LiO_2^* \rightleftharpoons Li^+_{(sol)} + O_2^-{}_{(sol)}$ + ion pairs + higher aggregates (clusters). The morphology of Li_2O_2 has been related to the solvent donor number. In the intermediate donor number ethers, both electrode surface and solution pathways contribute significantly and simultaneously to Li_2O_2 formation at high voltages, leading to significant Li_2O_2 surface films and particles in solution. Low donor number solvents lead to Li_2O_2 film growth, decaying rates, low capacities and early cell death. In contrast, in high donor number solvents the dominance of Li_2O_2 particle growth in solution leads to sustained discharge and higher capacities, encouraging the search for new, sufficiently stable, high donor number solvents.

ACKNOWLEDGEMENTS

P.G.B. is indebted to the EPSRC including the SUPERGEN program for financial support. S.A.F. acknowledges financial support by the Austrian Federal Ministry of Economy, Family and Youth and the Austrian National Foundation for Research, Technology and Development. We also thank Prof. D. Larcher for useful discussions.

NOTES

‡These authors contributed equally to this work. L.J. and C.L. designed and performed electrochemical and Raman spectroscopy experiments and analyzed the data. Z.L. discharged and performed microscopy of Li_2O_2 on high surface area cathodes. P.C.A. and

B.B.P. built and maintained the Raman microscope and contributed to the Raman measurements and analysis. Y.C. performed the UV-vis spectroscopy experiments and analyzed the data. P.G.B, L.J., Y. C., S. F. interpreted the data. P.G.B. wrote the paper with contributions from L.J.. P.G.B., J-M.T., K.D. supervised the project.

MATERIALS AND METHODS

Please refer to the Supplementary Information for details of the Materials and Methods.

REFERENCES

1. Black R, Adams B, Nazar LF. Non-Aqueous and Hybrid Li-O2 Batteries. *Adv Energy Mater* 2012, **2**(7)**:** 801-815.
2. Bruce PG, Freunberger SA, Hardwick LJ, Tarascon J-M. Li-O2 and Li-S batteries with high energy storage. *Nat Mater* 2012, **11**(1)**:** 19-29.
3. Choi N-S, Chen Z, Freunberger SA, Ji X, Sun Y-K, Amine K*, et al.* Challenges Facing Lithium Batteries and Electrical Double-Layer Capacitors. *Angew Chem Int Edit* 2012, **51**(40)**:** 9994-10024.
4. Shao YY, Park S, Xiao J, Wang Y, Liu J, Zhang JG. Electrocatalysts for Nonaqueous Lithium-Air Batteries: Status, Challenges, and Perspective. *ACS Catal* 2012, **2**(5)**:** 844-857.
5. Thackeray MM, Chan MKY, Trahey L, Kirklin S, Wolverton C. A Vision for Designing High Energy, Hybrid Li-Ion/Li-O2 Cells. *J Phys Chem Lett* 2013, **4**(21)**:** 3607-3611.
6. Girishkumar G, McCloskey B, Luntz AC, Swanson S, Wilcke W. Lithium - Air Battery: Promise and Challenges. *J Phys Chem Lett* 2010, **1**(14)**:** 2193-2203.
7. Lu Y-C, Gallant BM, Kwabi DG, Harding JR, Mitchell RR, Whittingham MS*, et al.* Lithium-Oxygen Batteries: Bridging Mechanistic Understanding and Battery Performance. *Energ Environ Sci* 2013, **6**(3)**:** 750-768.
8. Garcia-Araez N, Novák P. Critical aspects in the development of lithium–air batteries. *J Solid State Electrochem* 2013, **17**(7)**:** 1793-1807.
9. Li F, Zhang T, Zhou H. Challenges of non-aqueous Li-O2 batteries: electrolytes, catalysts, and anodes. *Energ Environ Sci* 2013, **6**(4)**:** 1125-1141.
10. Wang Z-L, Xu D, Xu J-J, Zhang X-B. Oxygen electrocatalysts in metal-air batteries: from aqueous to nonaqueous electrolytes. *Chem Soc Rev* 2014, **DOI: 10.1039/C3CS60248F**.
11. McCloskey BD, Scheffler R, Speidel A, Girishkumar G, Luntz AC. On the Mechanism of Nonaqueous Li–O2 Electrochemistry on C and Its Kinetic Overpotentials: Some Implications for Li–Air Batteries. *J Phys Chem C* 2012, **116**(45)**:** 23897-23905.
12. Viswanathan V, Nørskov JK, Speidel A, Scheffler R, Gowda S, Luntz AC. Li–O2 Kinetic Overpotentials: Tafel Plots from Experiment and First-Principles Theory. *J Phys Chem Lett* 2013**:** 556-560.
13. Lu J, Lei Y, Lau KC, Luo X, Du P, Wen J*, et al.* A nanostructured cathode architecture for low charge overpotential in lithium-oxygen batteries. *Nat Commun* 2013, **4:** 2383.
14. Laoire CO, Mukerjee S, Abraham KM, Plichta EJ, Hendrickson MA. Influence of Nonaqueous Solvents on the Electrochemistry of Oxygen in the Rechargeable Lithium−Air Battery. *J Phys Chem C* 2010, **114**(19)**:** 9178-9186.
15. Allen CJ, Hwang J, Kautz R, Mukerjee S, Plichta EJ, Hendrickson MA*, et al.* Oxygen Reduction Reactions in Ionic Liquids and the Formulation of a General ORR Mechanism for Li-Air Batteries. *J Phys Chem C* 2012, **116**(39)**:** 20755-20764.

16. Trahan MJ, Mukerjee S, Plichta EJ, Hendrickson MA, Abraham KM. Studies of Li-Air Cells Utilizing Dimethyl Sulfoxide-Based Electrolyte. *J Electrochem Soc* 2013, **160**(2)**:** A259-A267.
17. Sharon D, Afri M, Noked M, Garsuch A, Frimer AA, Aurbach D. Oxidation of Dimethyl Sulfoxide Solutions by Electrochemical Reduction of Oxygen. *J Phys Chem Lett* 2013, **4**(18)**:** 3115-3119.
18. Herranz J, Garsuch A, Gasteiger HA. Using Rotating Ring Disc Electrode Voltammetry to Quantify the Superoxide Radical Stability of Aprotic Li–Air Battery Electrolytes. *J Phys Chem C* 2012, **116**(36)**:** 19084-19094.
19. Zhang T, Zhou H. A reversible long-life lithium–air battery in ambient air. *Nat Commun* 2013, **4:** 1817.
20. Walker W, Giordani V, Uddin J, Bryantsev VS, Chase GV, Addison D. A Rechargeable Li-O2 Battery Using A Lithium Nitrate/N,N-Dimethylactamide Electrolyte. *J Am Chem Soc* 2013, **135**(6)**:** 2076–2079.
21. Adams BD, Radtke C, Black R, Trudeau ML, Zaghib K, Nazar LF. Current density dependence of peroxide formation in the Li-O2 battery and its effect on charge. *Energ Environ Sci* 2013, **6**(6)**:** 1772-1778.
22. Hummelshoj JS, Luntz AC, Norskov JK. Theoretical evidence for low kinetic overpotentials in Li-O2 electrochemistry. *J Chem Phys* 2013, **138**(3)**:** 034703-034712.
23. Jung HG, Hassoun J, Park JB, Sun YK, Scrosati B. An improved high-performance lithium-air battery. *Nat Chem* 2012, **4**(7)**:** 579-585.
24. Mitchell RR, Gallant BM, Shao-Horn Y, Thompson CV. Mechanisms of Morphological Evolution of Li2O2 Particles During Electrochemical Growth. *J Phys Chem Lett* 2013, **4**(7)**:** 1060–1064.
25. Nasybulin E, Xu W, Engelhard M, Nie Z, Burton SD, Cosimbescu L*, et al.* Effects of Electrolyte Salts on the Performance of Li-O2 Batteries. *J Phys Chem C* 2013, **117**(6)**:** 2635-2645.
26. Nasybulin E, Xu W, Engelhard MH, Li XS, Gu M, Hu D*, et al.* Electrocatalytic properties of poly(3,4-ethylenedioxythiophene) (PEDOT) in Li-O2 battery. *Electrochem Commun* 2013, **29**(0)**:** 63-66.
27. Kang S, Mo Y, Ong SP, Ceder G. A facile mechanism for recharging Li2O2 in Li-O2 batteries. *Chem Mater* 2013, **25**(16)**:** 3328–3336.
28. Suntivich J, Gasteiger HA, Yabuuchi N, Nakanishi H, Goodenough JB, Shao-Horn Y. Design principles for oxygen-reduction activity on perovskite oxide catalysts for fuel cells and metal-air batteries. *Nat Chem* 2011, **3**(7)**:** 546-550.
29. Younesi R, Hahlin M, Björefors F, Johansson P, Edström K. Li-O2 Battery Degradation by Lithium Peroxide (Li2O2): a model study. *Chem Mater* 2013, **25**(1)**:** 77–84.
30. Trahey L, Karan NK, Chan MKY, Lu J, Ren Y, Greeley J*, et al.* Synthesis, Characterization, and Structural Modeling of High-Capacity, Dual Functioning MnO2 Electrode/Electrocatalysts for Li-O2 Cells. *Adv Energy Mater* 2013, **3**(1)**:** 75-84.
31. Guo Z, Zhou D, Dong X, Qiu Z, Wang Y, Xia Y. Ordered Hierarchical Mesoporous/Macroporous Carbon: A High Performance Catalyst for Rechargeable Li–O2 batteries. *Adv Mater* 2013, **25**(39)**:** 5668–5672.
32. Li L, Manthiram A. Dual-electrolyte lithium-air batteries: influence of catalyst, temperature, and solid-electrolyte conductivity on the efficiency and power density. *J Mater Chem A* 2013, **1**(16)**:** 5121-5127.
33. Zhang T, Imanishi N, Shimonishi Y, Hirano A, Takeda Y, Yamamoto O*, et al.* A novel high energy density rechargeable lithium/air battery. *Chem Commun* 2010, **46**(10)**:** 1661-1663.
34. Xu J-J, Wang Z-L, Xu D, Zhang L-L, Zhang X-B. Tailoring deposition and morphology of discharge products towards high-rate and long-life lithium-oxygen batteries. *Nat Commun* 2013, **4:** 2438.

35. Younesi R, Hahlin M, Treskow M, Scheers J, Johansson P, Edström K. Ether Based Electrolyte, LiB(CN)4 Salt and Binder Degradation in the Li–O2 Battery Studied by Hard X-ray Photoelectron Spectroscopy (HAXPES). *J Phys Chem C* 2012, **116**(35)**:** 18597-18604.
36. Yang J, Zhai D, Wang H-H, Lau KC, Schlueter JA, Du P*, et al.* Evidence for lithium superoxide-like species in the discharge product of a Li-O2 battery. *Phys Chem Chem Phys* 2013, **15**(11)**:** 3764-3771.
37. Lu J, Qin Y, Du P, Luo X, Wu T, Ren Y*, et al.* Synthesis and characterization of uniformly dispersed Fe3O4/Fe nanocomposite on porous carbon: application for rechargeable Li-O2 batteries. *RSC Advances* 2013, **3**(22)**:** 8276-8285.
38. Veith GM, Nanda J, Delmau LH, Dudney NJ. Influence of Lithium Salts on the Discharge Chemistry of Li–Air Cells. *J Phys Chem Lett* 2012, **3**(10)**:** 1242-1247.
39. Pearson RG. Hard and Soft Acids and Bases. *J Am Chem Soc* 1963, **85**(22)**:** 3533-&.
40. Sawyer DT, Chlericato G, Angelis CT, Nanni EJ, Tsuchiya T. Effects of Media and Electrode Materials on the Electrochemical Reduction of Dioxygen. *Anal Chem* 1982, **54**(11)**:** 1720-1724.
41. Vasudevan D, Wendt H. Electroreduction of oxygen in aprotic media. *J Electroanal Chem* 1995, **392**(1–2)**:** 69-74.
42. Nissim R, Batchelor-McAuley C, Li Q, Compton RG. The anthraquinone mediated one-electron reduction of oxygen in acetonitrile. *J Electroanal Chem* 2012, **681**(0)**:** 44-48.
43. Laoire CO, Mukerjee S, Abraham KM, Plichta EJ, Hendrickson MA. Elucidating the Mechanism of Oxygen Reduction for Lithium-Air Battery Applications. *J Phys Chem C* 2009, **113**(46)**:** 20127-20134.
44. Lu YC, Gasteiger HA, Parent MC, Chiloyan V, Shao-Horn Y. The Influence of Catalysts on Discharge and Charge Voltages of Rechargeable Li-Oxygen Batteries. *Electrochem Solid-State Lett* 2010, **13**(6)**:** A69-A72.
45. Bard AJ, Faulkner LR. *Electrochemical Methods: Fundamentals and Applications*, 2nd edn. John Wiley & Sons, 2001.
46. Peng Z, Freunberger SA, Hardwick LJ, Chen Y, Giordani V, Bardé F*, et al.* Oxygen Reactions in a Non-Aqueous Li+ Electrolyte. *Angew Chem Int Edit* 2011, **50**(28)**:** 6351-6355.
47. Pasgreta E, Puchta R, Galle M, Hommes NvE, Zahl A, van Eldikal R. Ligand-exchange processes on solvated lithium cations: DMSO and water/DMSO mixtures. *Chemphyschem* 2007, **8**(9)**:** 1315-1320.
48. Bryantsev V. Calculation of solvation free energies of Li+ and O2 − ions and neutral lithium–oxygen compounds in acetonitrile using mixed cluster/continuum models. *Theor Chem Acc* 2012, **131**(7)**:** 1-11.
49. Das U, Lau KC, Redfern PC, Curtiss LA. Structure and Stability of Lithium Superoxide Clusters and Relevance to Li-O-2 Batteries. *J Phys Chem Lett* 2014, **5**(5)**:** 813-819.
50. Bryantsev VS, Giordani V, Walker W, Blanco M, Zecevic S, Sasaki K*, et al.* Predicting Solvent Stability in Aprotic Electrolyte Li-Air Batteries: Nucleophilic Substitution by the Superoxide Anion Radical (O-2(center dot-)). *J Phys Chem A* 2011, **115**(44)**:** 12399-12409.
51. Bryantsev VS, Blanco M, Faglioni F. Stability of Lithium Superoxide LiO2 in the Gas Phase: Computational Study of Dimerization and Disproportionation Reactions. *J Phys Chem A* 2010, **114**(31)**:** 8165-8169.
52. Horstmann B, Gallant B, Mitchell R, Bessler WG, Shao-Horn Y, Bazant MZ. Rate-Dependent Morphology of Li2O2 Growth in Li–O2 Batteries. *J Phys Chem Lett* 2013, **4**(24)**:** 4217-4222.
53. Luntz AC, Viswanathan V, Voss J, Varley JB, Norskov JK, Scheffler R*, et al.* Tunneling and Polaron Charge Transport Through Li2O2 in Li-O2 Batteries. *J Phys Chem Lett* 2013, **4**(20)**:** 3494–3499.